SCIENTIFIC REPORTS

OPEN

SUBJECT AREAS:
SUPRAMOLECULAR ASSEMBLY
BIOINSPIRED MATERIALS

Received
28 July 2014

Accepted
19 November 2014

Published
5 December 2014

Correspondence and requests for materials should be addressed to J.P.-R. (jperez@mater.upm.es)

Spider silk gut: Development and characterization of a novel strong spider silk fiber

Ping Jiang[1,2], Núria Marí-Buyé[2,3], Rodrigo Madurga[2,3], María Arroyo-Hernández[2,3], Concepción Solanas[2,3], Alfonso Gañán[4], Rafael Daza[2,3], Gustavo R. Plaza[2,3], Gustavo V. Guinea[2,3], Manuel Elices[2,3], José Luis Cenis[5] & José Pérez-Rigueiro[2,3]

[1]College of Life Sciences, Jinggangshan University, Jiangxi Province, Ji'an, 343009, China, [2]Centro de Tecnología Biomédica. Universidad Politécnica de Madrid. 28223 Pozuelo de Alarcón (Madrid). Spain, [3]Departamento de Ciencia de Materiales. ETSI Caminos, Canales y Puertos. Universidad Politécnica de Madrid. 28040. Madrid. Spain, [4]Escuela Técnica Superior de Ingenieros. Universidad de Sevilla. 41092. Sevilla. Spain, [5]Instituto Murciano de Investigación y Desarrollo Agrario y Alimentario. 30150 La Alberca (Murcia). Spain.

Spider silk fibers were produced through an alternative processing route that differs widely from natural spinning. The process follows a procedure traditionally used to obtain fibers directly from the glands of silkworms and requires exposure to an acid environment and subsequent stretching. The microstructure and mechanical behavior of the so-called spider silk gut fibers can be tailored to concur with those observed in naturally spun spider silk, except for effects related with the much larger cross-sectional area of the former. In particular spider silk gut has a proper ground state to which the material can revert independently from its previous loading history by supercontraction. A larger cross-sectional area implies that spider silk gut outperforms the natural material in terms of the loads that the fiber can sustain. This property suggests that it could substitute conventional spider silk fibers in some intended uses, such as sutures and scaffolds in tissue engineering.

The essential traits of spider silk fibers[1] and of their constituent elements, spidroin proteins[2], have been fixed in a series of sequential steps that started with the production of solid threads and culminated with the spinning of high performance fibers[3]. During this process, protein composition and spinning route evolved to yield the unique microstructure and properties of spider silk[4]. However, disentangling the individual contributions of the chemical structure of the proteins[5] and of the physiological and anatomical features related to fiber processing[6], has proven an extremely involved task that severely hampers a possible biomimetic[7] approach based on these materials[8,9].

An alternative to the natural spinning process exists for the production of silkworm silk fibers. This processing route is based on a traditional procedure that allows obtaining fibers directly from the glands of the worms after being exposed to an acid environment and subsequently stretched[10,11], yielding the so-called silkworm silk gut fibers. Following this technique, it is shown that high-performance spider silk gut fibers can also be produced directly from the major ampullate gland of orb-web weaving spiders.

Major ampullate gland as dissected from the spider shows a mucus-like texture and breaks up readily if stretched while being held with tweezers. Similar behavior is observed if the gland is incubated in neutral or slightly basic solutions prior to stretching. In contrast, if incubated in an acid environment (acetic acid/water), a solid fiber is obtained upon stretching. The morphology of spider silk guts, including fracture surfaces of tensile tested samples, is shown in Figure 1. These images do not show any remains of the gland tissues on the fiber, which are assumed to play no significant role in the process. A wide range of diameters from 30 μm to 240 μm were found in the fibers, and significant variability was observed even along individual fibers. The diameter in the middle region of each fiber was systematically greater than those at the ends. Different diameters were typically measured at both ends of a given fiber, possibly reflecting initial variations in the diameter of the original gland. Longer incubation times usually led to increased values of the average diameter of the fiber. Fracture surfaces appeared flat with no evidence of the presence of a fibrillar microstructure at the micrometer scale.

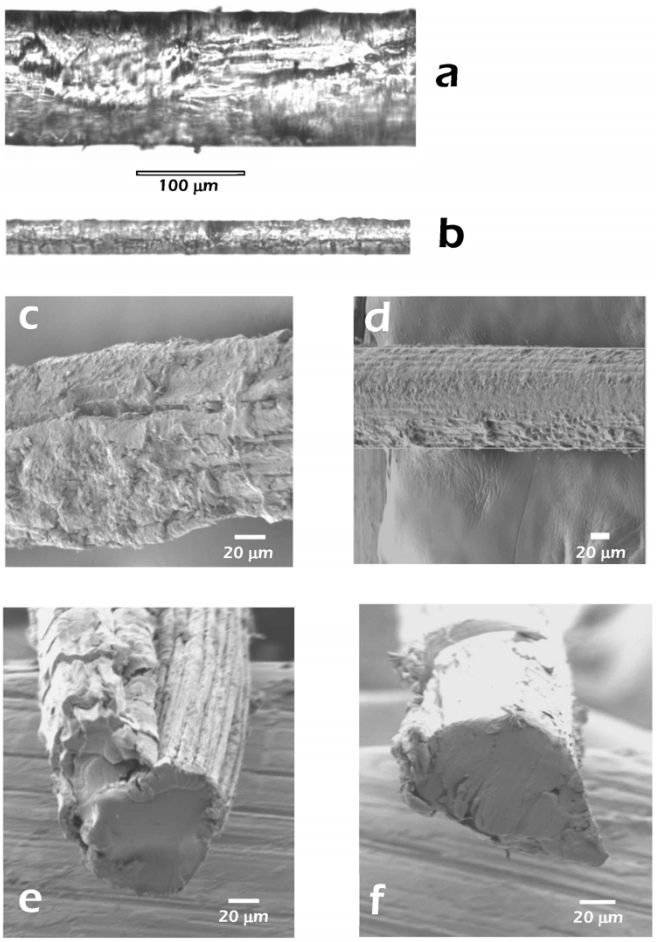

Figure 1 | Representative spider silk gut micrographs. (a) and (b) optical micrographs. (c) and (d) SEM micrographs of the lateral surface. (e) and (f) SEM micrographs of fracture surfaces. Scale is indicated in each micrograph.

During natural spinning, shear stresses are expected to induce conformational changes in the soluble fibroins that lead to the formation of β-nanocrystallites and result in the formation of insoluble fibers[12]. pH is considered to play a role in the formation process due to the presence of proton pumps in the gland[13] and of pH-sensitive domains in spidroins[14,15]. The results obtained on spider silk gut not only confirm these basic assumptions but also allow a quantitative description of the process.

Thus, it is found that the silk gut is formed exclusively by the combined action of an acid environment and subsequent stretching. The process is sensitive to the acid concentration, with an optimal 1% acetic acid/water (v/v) solution being found for an incubation time of three minutes. Higher concentrations led to a faster solidification of the gland, preventing any subsequent change induced by stretching. Concentrations below 0.5% did not lead to fiber formation. The use of the optimal conditions was found to ensure not only a high reproducibility of the silk gut properties but also the concurrence of its mechanical properties with those of natural major ampullate (MA) silk fibers. Longer incubation times led to an increase in the variability of the material, with a trend towards stiffer fibers being apparent. No significant differences were observed among fibers stretched at different speeds.

The forces and strains involved in the process were monitored during fiber formation (Figure 2). Strain is defined as the ratio between the increase in length of the gland and its initial length fixed at 5 mm. No clear trends were found between the measured forces and incubation time or stretching speed. Conversion of the forces into stresses during the process requires careful consideration of the cross-sectional area to be used. Thus, it was found that the apparent diameters in the middle of a single fiber could be up to three times greater than the values observed at the ends (acetic acid concentration: 1%; incubation time: six minutes from 93 to 240 μm; Acetic acid concentration: 1%, incubation time: six minutes from 32 to 110 μm). It was also found that the values at the ends of a given fiber, albeit smaller than those in the middle, were not necessarily similar. These differences might possibly reflect initial variations in the diameter of the original gland.

Since the most relevant parameter of the formation process is the minimum stress required to complete the transition from the viscous fluid to the solid fiber, formation stresses were calculated by using the value of the maximum cross section measured on the fiber. Four samples were produced under optimal incubation conditions and stretched to the point that elongations of either 30 mm or 40 mm were reached. These processes allow estimating a value of approximately 700 kPa for the formation stresses, although the actual value required to form the fiber might be significantly lower, since fibers were formed before stopping the process.

Previous quantitative estimates of the silking stresses had been obtained by either analysing the rheological behavior of the protein solution in the gland[16,17] or by direct measurement of the forces involved in the forced silking process[18]. Values of approximately 40 MPa were consistently reported, with these relatively high values being interpreted as an indication of the importance of the silking stresses in the fiber formation process. In contrast, the stresses required for forming silk gut fibers are found to be significantly lower. This discrepancy suggests that stress on its own does not seem to be the ultimate mechanism that controls fiber formation. Instead, fiber formation seems to require the relative displacement among the proteins which, in turn, induce conformational changes of the protein chains and finally lead to the creation of β-nanocrystallites. Although this reorganization is induced by mechanical stresses, comparison of natural MA and silk gut indicates that different processing systems may yield the same material regardless of the actual values of the stresses required in each case.

Representative Fourier transform infrared (FTIR) spectra and X-ray diffraction (XRD) patterns of spider silk guts are shown in Figure 3. The region of the amide I and amide II peaks are presented in Figure 3a and compared with a spectrum of *Nephila inaurata* MA silk. All spectra show concurring peaks at 1626 cm^{-1} and 1514 cm^{-1}, that are associated with a β-pleated secondary structure[19,20]. XRD patterns of silk guts show diffraction spots that can be assigned to the (210) and (010) planes of an orthorhombic unit cell with parameters $a = 0.96 \pm 0.07$ nm and $b = 1.06 \pm 0.06$ nm (Fig. 3d). The size of the nanocrystals and the fraction of crystalline phase were estimated from the patterns yielding values of ~3 nm and $\chi \sim 18\%$, respectively. The position of the diffraction spots, dimensions of the unit cell, size of the nanocrystals and crystalline fraction are all comparable with values previously reported from maximum supercontracted *Argiope trifasciata* MA silk[21]. Microstructural data also show that the formation of spider silk gut is completed at the early stages of stretching.

The concurring mechanical behavior of silk guts and MA is observed from the comparison of their tensile properties when tested in water (Figure 4a), which suggests a common mechanism controlled by forces of entropic origin[22,23] to both sets of fibers. Concurrent behaviour in water suggests that there is a possible existence of a ground state in silk gut[24] to which the fiber can return regardless of its loading history, with it being manifested through supercontraction[25] in water. All silk guts showed supercontraction with values of the percentage of supercontraction[24] (%SC) ranging from % SC = 9% to % SC = 46%. No clear trend was established between the formation conditions and % SC. The existence of a

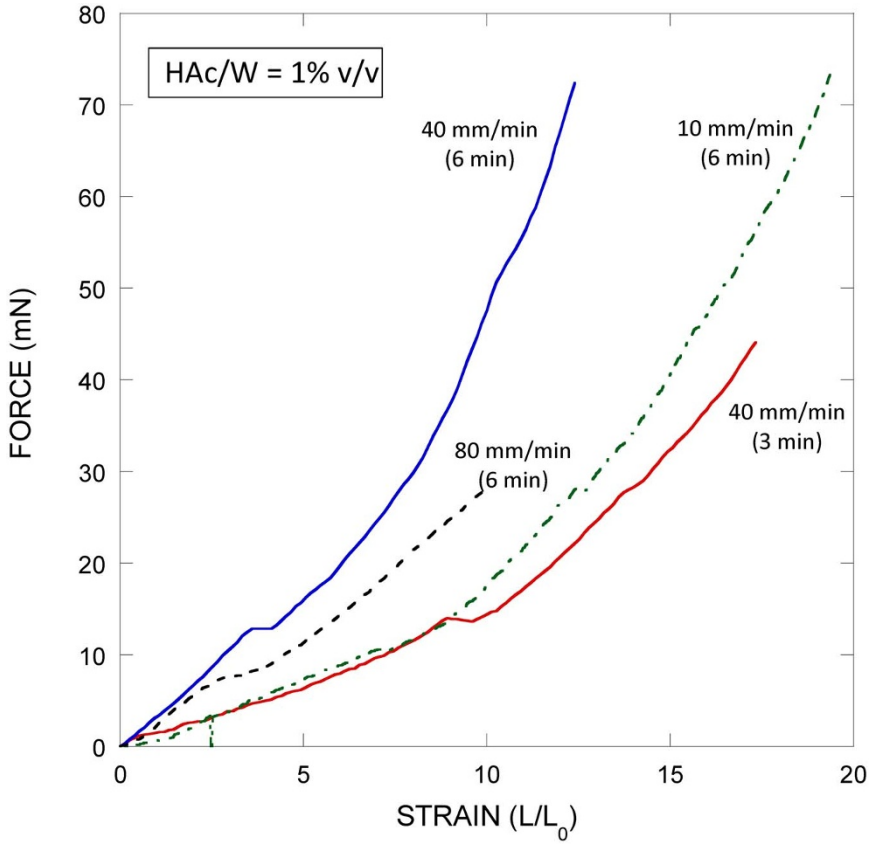

Figure 2 | Representative curves of the force exerted during spider silk gut formation vs strain. Base length, $L_0 = 5$ mm. All fibers were incubated in an acetic acid/water (1% v/v) solution. The values of the incubation time and stretching speed of each process are indicated.

ground state was further confirmed through recovery tests[26] (Figure 4b).

Maximum supercontracted spider guts and MA fibers were shown to yield concurring true stress-true strain curves (Figure 4c), even for the samples prepared with the lowest strain values (curve marked *). Although some curves of the samples incubated for six minutes concurred with those of MA silk (curve marked **), variability was shown to increase with incubation time as most fibers showed a stiffer behaviour. The existence of a ground state even in the stiffest fibers was proved through recovery tests. This finding suggests that different ground states can be shaped in spider silk during processing and remain imprinted in the fiber independently from its subsequent loading history.

The major difference in mechanical behaviour between silk gut and MA silk is the lower values of tensile stress and strain at breaking of the former. Three possible causes might account for this difference: i) unobserved microstructural differences between each material, ii) the inhomogeneous cross-sectional area of silk guts, and iii) their larger cross-sectional areas.

Although some differences in the microstructures of each material cannot be completely discarded, it is apparent that inhomogeneities will lead to the appearance of stress concentration sites in the regions where the cross-sectional area varies, with the subsequent reduction in the mechanical properties of silk gut. In addition, it is a general trend in fiber science that the resistance of any given material increases when the cross-sectional area of the fiber decreases[27]. In this regard, the detailed comparison of the breaking behavior of MA and silk gut shows that the latter presents an unexpected tensile strength. The estimated value of the mean tensile strength of silk gut can be calculated by following a Weibull analysis from the values of the Weibull parameter, the mean tensile strength of MA silk and the cross-sectional areas of each type of fibers as: $\bar{\sigma}_{gut} \sim \left(\frac{S_{MA}}{S_{gut}}\right)^{1/m} \bar{\sigma}_{MA}$. Assuming values of $m = 3.4$[28] for the Weibull parameter, $\bar{\sigma}_{MA} \sim 1200$ MPa for the mean tensile strength of MA fibers, and $S_{MA} \sim 4\ \mu m^2$ and $S_{gut} \sim 40000\ \mu m^2$ for the cross-sectional areas of spider silk and silk gut, respectively, the predicted value of the mean tensile strength of silk gut is $\bar{\sigma}_{gut} \sim 80$ MPa far below the experimental value of $\bar{\sigma}_{gut} \sim 450$ MPa.

Finally, and although a larger cross-sectional area probably reduces its tensile strength, such an area also endows spider silk gut with the possibility of sustaining forces of hundreds of grams in contrast to the forces in the order of grams sustained by MA fibers. In particular, the fiber marked (**) in Figure 4c reached the maximum value of breaking force (5500 mN) of all silk guts. Following the previous discussion, this particular fiber can surely claim the honour to have sustained the highest load a spider silk fiber has ever managed. A deeper knowledge of the spider silk gut system will probably make this moment of glory ephemeral.

Methods

Spider silk guts were prepared from MA silk glands of adult female *Nephila inaurata* spiders (Fig. 5a). Prior to gland retrieval, the spiders were kept in captivity and fed a diet of crickets. The glands were dissected from anaesthetized spiders and kept in Ringer's solution for a period not exceeding 25 minutes before starting the spider silk gut formation process. Care was taken to extract specifically major ampullate silk glands[29,30] in a way that the glands were not broken during dissection.

Spider silk gut formation started with the transfer of MA glands from the Ringer's solution to an acetic acid/water solution (Fig. 5b). From a set of preliminary tests, values of acetic acid concentration of 0.5% (pH = 2,9) or 1% in water (v/v) (pH = 2,6) and durations of either three or six minutes were used. After removal from the acetic acid solution, glands were stretched in a tensile testing machine (Instron 4411) (Fig. 5c). A balance AND 1200 (resolution ± 10 mg) was used to measure the force exerted on the gland during stretching, as described elsewhere[31]. Self-closing tweezers were used as upper and lower grips for silk gut formation. A droplet of glue was deposited on the tip of the tweezers to improve hold. The gland was positioned with

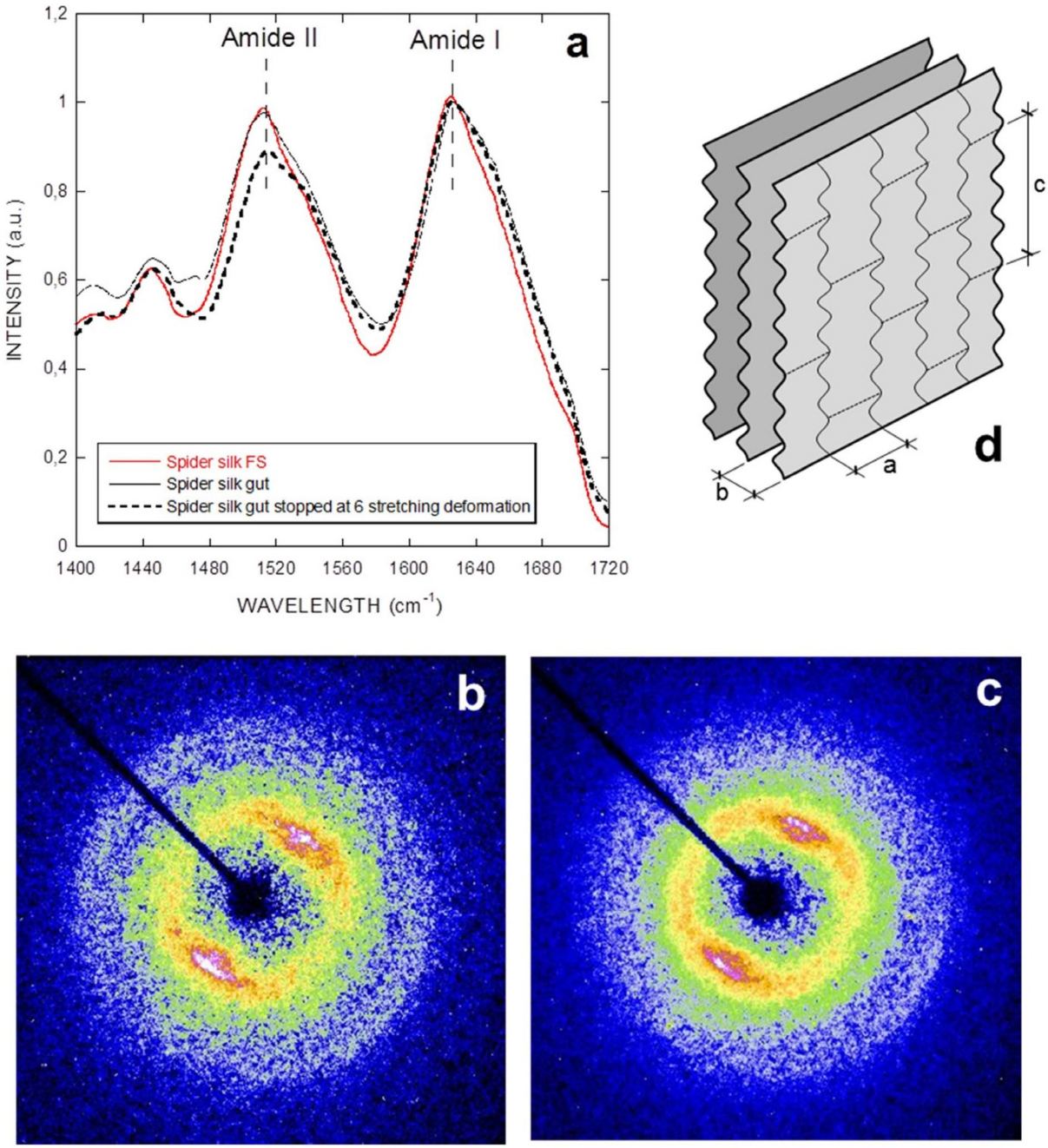

Figure 3 | Microstructural characterization of spider silk gut. (a) FTIR spectra of the amide I and amide II region of spider silk guts obtained either after fully stretching or after controlled stretching up to a deformation of 30 mm (initial length of the gland, L_0 = 5 mm). The FTIR spectrum of a *Nephila inaurata* MA silk fiber obtained by forced silking is shown for comparison. All spectra are normalized using the value of the intensity at 1625 cm^{-1} (amide I peak). (b) and (c) XRD diffraction patterns of spider silk guts either fully stretched or after controlled stretching up to a deformation of 30 mm, respectively. (d) A scheme of a β-nanocrystals indicating the labelling of the unit cell dimensions.

its middle portion approximately located between the tweezers, with the tips being kept at a distance of 5 mm. Stretching of the gland proceeded in air at speeds of 10, 40 and 80 mm/min until it became detached from one of the tips of the tweezers. A small number of samples which could not be held properly with the tweezers were stretched manually.

Each spider silk gut was cut into a number of adjacent samples with an approximate length of 30 mm (Fig. 5d). The number of samples depended on the initial length of the silk gut and ranged from one to four. The lateral dimensions of all the samples were measured from optical micrographs recorded with an optical microscope (Leica DMI 3000 B). At least four micrographs were taken from each sample and at least two measurements were taken from each micrograph using the ImageJ program. After tensile testing, the samples were retrieved, metallized with gold for 45 seconds and observed in a field emission scanning electron microscopy (FESEM) Auriga Zeiss at V = 3 kV.

Before tensile testing, all the samples were subjected to maximum supercontraction in order to reduce the intrinsic variability observed in the silks[32,33]. Samples were allowed to supercontract for four hours in water (Fig. 5e) and then dried overnight before being subjected to any additional test. The extent of supercontraction was measured with the percentage of supercontraction, %SC, defined as $\%SC = 100 \times (L_0 - L_{MS})/L_0$ where L_0 is the initial length of the fiber and L_{MS} is the length after maximum supercontraction.

The mechanical properties of maximum supercontracted silk guts were studied by means of tensile tests performed in air or water (Fig. 5f). Tensile tests in air were performed at a speed of 1 mm/min. Loads exerted on the fibers were measured with a balance AND 1200, with it being assumed that the displacement of the upper grip was a sufficiently accurate measurement of the increase of length of the sample, since the compliance of the fiber was much larger than that of the rest of the experimental setup[31]. Tensile tests in air proceeded at nominal conditions T = 23°C and relative humidity 40%. Tensile tests in water were performed at a speed of 1 mm/min. Samples were maintained immersed in water for at least four hours before starting the test.

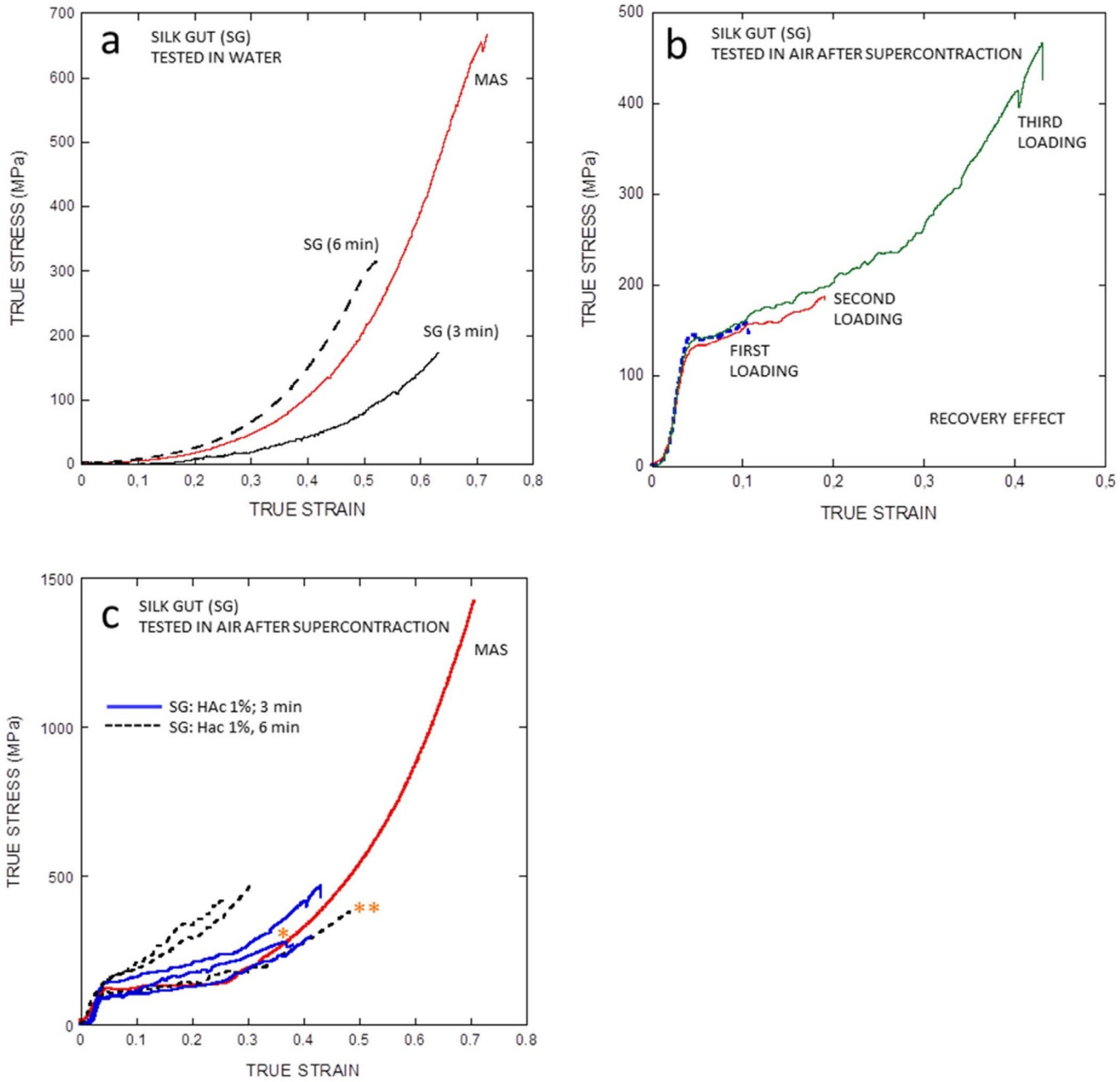

Figure 4 | Tensile properties of spider silk gut. (a) True stress-true strain curves of spider silk guts tested in water. Both samples were incubated in 1% (v/v) acetic acid/water solution for either 3 minutes (solid line) or 6 minutes (broken line). The behavior of *Nephila inaurata* MA silk tested in water, labelled as MAS, is shown for comparison. (b) Recovery test of spider silk gut. A spider silk gut was subjected to three consecutive steps of stretching in air, unloading (not shown in the Figure) and maximum supercontraction. The true stress-true strain curves measured after maximum supercontraction are shown to concur. The third step proceeded until the breaking of the fiber. (c) True stress-true strain curves of spider silk guts prepared under different conditions. The true stress-true strain curve of a maximum supercontracted *Nephila inaurata* MA fiber is shown for comparison and labelled as MAS. All samples incubated for 3 minutes in a 1% (v/v) acetic acid/water solution yield concurring curves with the MAS curve up to the breaking point (solid blue curves). The curve marked with * corresponds to spider silk gut formed by stretching the gland up to a final strain of 7. Samples incubated for longer incubation times (6 minutes) showed a greater variability, ranging from curves concurring with those of MAS (dashed curve marked **) to curves significantly stiffer than that of MAS.

Force-displacement curves were converted into true stress-true strain curves by using cross-sectional areas calculated from the lateral dimensions obtained from the optical micrographs assuming a circular cross section. True strain, ε, was calculated as $d\varepsilon = dL/L$, which leads to the expression $\varepsilon = \ln(1 + e)$, where e is engineering strain defined as $e = (L - L_0)/L_0$, and L_0 and L are the initial and instantaneous length of the sample, respectively. True strain was calculated as $\sigma = F/A$, where A is the instantaneous area of the fiber. The instantaneous area of the fiber was calculated as $A = A_0L_0/L$ from the initial area, A_0, as obtained from the optical microscope (SEM) measurements under the constant volume hypothesis[34]. Since optical micrographs were taken of the samples before supercontraction, the cross-sectional areas of the samples after supercontraction were calculated by assuming again that the volume of the fibers remains constant throughout the supercontraction process[34].

However, the large variability of the lateral dimensions of any given sample requires careful consideration of the area used for conversion of forces into stresses. Thus, usage of an average diameter on samples with large variations in their cross-sectional areas implies overestimating the stresses on the thicker sections and underestimating those in the thinner ones. In contrast, usage of the minimum diameter allows the accurate determination of the stresses exerted on the thinnest sections which, in turn, corresponds to the maximum stresses exerted on the fiber. Using the minimum diameter has the drawback of overestimating the stress of the thicker

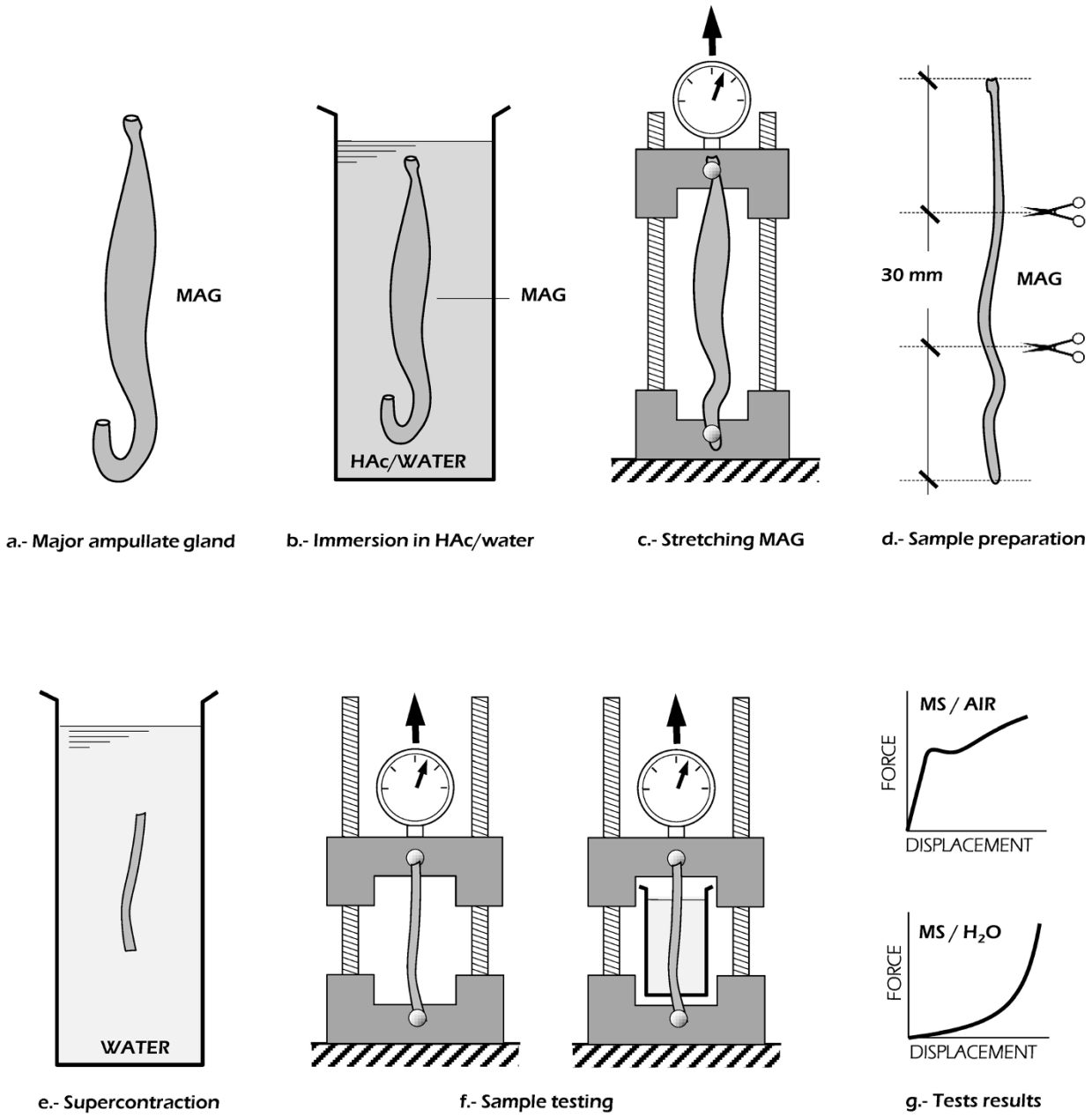

Figure 5 | Scheme of the formation process of spider silk gut. (a) retrieval of the gland, (b) immersion in acetic acid solution, (c) stretching, (d) sample cutting, (e) maximum supercontraction of the fiber, (f and g) tensile testing in air or in water.

portions of the sample which, consequently, implies overestimating the stiffness of the sample. At the very least, however, it could be argued that true stress-true strain curves obtained from the minimum value of the cross-sectional area yield an upper limit of the actual true stress-true strain curves of the material and the correct tensile strength.

The microstructure of spider silk guts processed under distinct conditions was studied by attenuated total reflection Fourier transform infrared (ATR-FTIR) and X-ray diffraction (XRD). ATR-FTIR spectra were obtained in the range 550–4000 cm^{-1} in a Nicolet iS5 FT-IR with ATR module under observation conditions: 64 scans per spectrum with a resolution of 4 cm^{-1}. XRD was performed at room temperature in a Bruker Smart 1000 CCD diffractometer by using graphite-monochromated Mo-Kα radiation (λ = 0.71073 Å) operating at 50 kV and 30 mA. Each still exposure was taken with a variable time that ranged from 100 to 800 seconds depending on the diameter of the fiber. Sample-to-detector distance was calibrated with Si powder (NIST SRM640d). Patterns with no sample were used as background and subtracted from the patterns of the fibers. An average of two images was made for each sample. A region containing the main equatorial reflections (020) and (210) was azimuthally integrated, resulting in a 1D profile. This profile was fitted with Gaussian functions for Bragg peaks and a short-range order halo, and a constant value for the residual background scattering of the sample[35].

The position of the Gaussian functions which correspond to the (020) and (210) reflections were used to calculate the unit cell parameters a and b of the β-sheet nanocrystals, which correspond to the interchain (hydrogen bonding) and the intersheet (piling-up of β-sheets) directions, respectively. Calculation assumed an orthorhombic geometry of the unit cell[36] and was based on Bragg's equation $n\lambda = 2d\sin\theta$. XRD-patterns were used to calculate the size of the nanocrystals and fraction of the crystalline phase as explained elsewhere[21].

1. Blackledge, T. A. *et al.* Sequential origin in the high performance properties of orb spider dragline silk. *Sci. Rep.* **2**, 782 (2012).
2. Gatesy, J., Hayashi, C., Motriuk, D., Woods, J. & Lewis, R. Extreme diversity, conservation, and convergence of spider silk fibroin sequences. *Science* **291**, 2603–2605 (2001).
3. Selden, P. A., Shear, W. A. & Sutton, M. D. Fossil evidence for the origin of spider spinnerets, and a proposed arachnid order. *Proc. Natl. Acad. Sci. U. S. A.* **105**, 20781–20785 (2008).
4. Heim, M., Keerl, D. & Scheibel, T. Spider silk: from soluble protein to extraordinary fiber. *Angew. Chem. Int. Ed Engl.* **48**, 3584–96 (2009).
5. Hayashi, C. Y., Shipley, N. H. & Lewis, R. V. Hypotheses that correlate the sequence, structure, and mechanical properties of spider silk proteins. *Int. J. Biol. Macromol.* **24**, 271–275 (1999).

6. Vollrath, F. & Knight, D. P. Liquid crystalline spinning of spider silk. *Nature* **410**, 541–548 (2001).
7. Gronau, G. *et al.* A review of combined experimental and computational procedures for assessing biopolymer structure-process-property relationships. *Biomaterials* **33** (2012).
8. Shao, Z. Z., Vollrath, F., Yang, Y. & Thogersen, H. C. Structure and behavior of regenerated spider silk. *Macromolecules* **36**, 1157–1161 (2003).
9. Scheibel, T. Spider silks: recombinant synthesis, assembly, spinning, and engineering of synthetic proteins. *Microb Cell Fact* **3**, 14 (2004).
10. Humphries, A. M. C. The story of silk and silkworm gut. *Post Graduate Medical Journal* **October**, 483–488 (1949).
11. Marden, L. Spain's silkworm gut. *National Geographic* **100**, 100–108 (1951).
12. Iizuka, E. Silk Thread - Mechanism of Spinning and its Mechanical-Properties. *Applied Polymer Symposia* **41**, 173–185 (1985).
13. Vollrath, F., Knight, D. P. & Hu, X. W. Silk production in a spider involves acid bath treatment. *Proc R Soc B* **265**, 817–820 (1998).
14. Askarieh, G. *et al.* Self-assembly of spider silk proteins is controlled by a pH-sensitive relay. *Nature* **465**, 236–239 (2010).
15. Hagn, F. *et al.* A conserved spider silk domain acts as a molecular switch that controls fibre assembly. *Nature* **465**, 239–242 (2010).
16. Holland, C., Terry, A. E., Porter, D. & Vollrath, F. Comparing the rheology of native spider and silkworm spinning dope. *Nature Materials* **5**, 870–874 (2006).
17. Kojic, N., Bico, J., Clasen, C. & McKinley, G. H. Ex vivo rheology of spider silk. *J. Exp. Biol.* **209**, 4355–4362 (2006).
18. Elices, M., Guinea, G. V., Plaza, G. R., Real, J. I. & Perez-Rigueiro, J. Example of microprocessing in a natural polymeric fiber: Role of reeling stress in spider silk. *J. Mater. Res.* **21**, 1931–1938 (2006).
19. Rousseau, M. E., Lefevre, T., Beaulieu, L., Asakura, T. & Pezolet, M. Study of protein conformation and orientation in silkworm and spider silk fibers using Raman microspectroscopy. *Biomacromolecules* **5**, 2247–2257 (2004).
20. Paquet-Mercier, F., Lefevre, T., Auger, M. & Pezolet, M. Evidence by infrared spectroscopy of the presence of two types of beta-sheets in major ampullate spider silk and silkworm silk. *Soft Matter* **9**, 208–215 (2013).
21. Plaza, G. R. *et al.* Relationship between microstructure and mechanical properties in spider silk fibers: two regimes in the microstructural changes. *Soft Matter* **8**, 6015–6026 (2012).
22. Gosline, J. M., Denny, M. W. & Demont, M. E. Spider Silk as Rubber. *Nature* **309**, 551–552 (1984).
23. Termonia, Y. in *Structural Biological Materials* (ed Elices, M.) 335–349 (Pergamon Press, Amsterdam, 2000).
24. Perez-Rigueiro, J., Elices, M. & Guinea, G. V. Controlled supercontraction tailors the tensile behaviour of spider silk. *Polymer* **44**, 3733–3736 (2003).
25. Work, R. W. Dimensions, Birefringences, and Force-Elongation Behavior of Major and Minor Ampullate Silk Fibers from Orb-Web-Spinning Spiders - Effects of Wetting on these Properties. *Text. Res. J.* **47**, 650–662 (1977).
26. Elices, M., Perez-Rigueiro, J., Plaza, G. & Guinea, G. V. Recovery in spider silk fibers. *J. Appl. Polym. Sci.* **92**, 3537–3541 (2004).
27. Chawla, K. K. in *Fibrous Materials* (Cambridge University Press, Cambridge, U.K., 1998).
28. Perez-Riguero, J., Elices, M., Llorca, J. & Viney, C. Tensile properties of Argiope trifasciata drag line silk obtained from the spider's web. *J Appl Polym Sci* **82**, 2245–2251 (2001).
29. Foelix, R. F. in *Biology of spiders* (Oxford University Press, Oxford, 2011).
30. Jeffery, F. *et al.* Microdissection of black widow spider silk-producing glands. *JoVE* **47**, 2382 (2011).
31. Perez-Rigueiro, J., Viney, C., Llorca, J. & Elices, M. Silkworm silk as an engineering material. *J Appl Polym Sci* **70**, 2439–2447 (1998).
32. Dunaway, D. L., Thiel, B. L. & Viney, C. Tensile Mechanical Property Evaluation of Natural and Epoxide-Treated Silk Fibers. *J Appl Polym Sci* **58**, 675–683 (1995).
33. Madsen, B., Shao, Z. Z. & Vollrath, F. Variability in the mechanical properties of spider silks on three levels: interspecific, intraspecific and intraindividual. *Int. J. Biol. Macromol.* **24**, 301–306 (1999).
34. Guinea, G. V., Perez-Rigueiro, J., Plaza, G. R. & Elices, M. Volume constancy during stretching of spider silk. *Biomacromolecules* **7**, 2173–2177 (2006).
35. Martel, A., Burghammer, M., Davies, R. J. & Riekel, C. Thermal Behavior of Bombyx mori silk: Evolution of crystalline parameters, molecular structure, and mechanical properties. *Biomacromolecules* **8**, 3548–3556 (2007).
36. Riekel, C. *et al.* Aspects of X-ray diffraction on single spider fibers. *Int. J. Biol. Macromol.* **24**, 179–186 (1999).

Acknowledgments

The spiders were reared in Reptilmadrid S.L. by Oscar Campos and Víctor Ruiz. The authors are grateful to José Miguel Martínez for his help with the artwork. The work was funded by Ministerio de Economía y Competitividad (Spain) through project MAT2012-38412-C02-01, by the Comunidad de Madrid (Spain) (Grant S2011/BMD-2460) and by Fundación Marcelino Botín. The stay of Dr. P. Jiang as visiting scholar supported by China Scholarship Council (CSC) at Centro de Tecnología Biomédica (Spain) was funded by the National Natural Sciences Fund of China (No. 31160420, 31060282, 30760041) and by the Training Program of Young Scientists (JingGang Star) in Jiangxi Province (No. 20133BCB23022).

Author contributions

J.P.R. proposed the experiments and wrote the main text. P.J. performed the dissections. N.M.B. and C.S. performed the infrared measurements and analysis of the spectra. R.M. and R.D. performed the analysis of the XRD data. M.A.H. prepared the samples and obtained the SEM micrographs. A.G., G.R.P., G.V.G., M.E. and J.L.C. contributed to the data analysis and reviewed the manuscript.

Additional information

Competing financial interests: The authors declare no competing financial interests.

How to cite this article: Jiang, P. *et al.* Spider silk gut: Development and characterization of a novel strong spider silk fiber. *Sci. Rep.* **4**, 7326; DOI:10.1038/srep07326 (2014).